ANALYSIS OF A WATER-COOLANT LEAK INTO A VERY HIGH-TEMPERATURE VITRIFICATION CHAMBER

Frank S. Felicione
Argonne National Laboratory - West
P.O. Box 2528
Idaho Falls, Idaho 83403
(208) 533-7547

ABSTRACT

A coolant-leakage incident occurred during *non*-radioactive operation of the Plasma Hearth Process waste-vitrification development system at Argonne National Laboratory when a stray electric arc ruptured a water-cooling jacket. Rapid evaporation of the coolant that entered the very high-temperature chamber pressurized the normally sub-atmospheric system above ambient pressure for over 13 minutes. Any positive pressurization, and particularly a lengthy one, is a safety concern since this can cause leakage of contaminants from the system.

A model of the thermal phenomena that describe coolant/hot-material interactions was developed to better understand the characteristics of this type of incident. The model is described and results for a variety of hypothetical coolant-leak incidents are presented. It is shown that coolant leak rates above a certain threshold will cause coolant to accumulate in the chamber, and evaporation from this pool can maintain positive pressure in the system long after the leak has been stopped. Application of the model resulted in reasonably good agreement with the duration of the pressure measured during the incident. A closed-form analytic solution is shown to be applicable to the initial leak period in which the peak pressures are generated, and is presented and discussed.

INTRODUCTION

Several new technologies that vitrify low-level mixed and transuranic wastes are under development. These melter systems necessarily involve very high temperatures, frequently produced by plasmas, electric arcs, or induction coils. Confinement of plutonium, other radionuclide contaminants, and hazardous materials is maintained by sub-atmospheric operation of the system upstream of off-gas HEPA filters, so that any leakage across the boundary is inward from the clean surroundings to the process. To protect the process equipment from the high temperatures and to minimize thermal distortion and stresses, water-cooling jackets are often employed. However, the presence of liquid coolants in equipment containing molten waste materials and, frequently, massive, very high-temperature refractory linings introduces significant safety concerns from potentially energetic interactions between coolant and hot materials, should any of the coolant be leaked into the system.

The contact of coolant on very hot surfaces can create a high-pressure shock wave, albeit of very limited duration. The magnitude of this pressure wave is important to structural evaluations, particularly for any attached filter enclosures, gloveboxes, etc. whose boundary constructions are usually not very stout. Shortly after the initial propagation, however, this pressure wave is fully dissipated. Thereafter, the continuing evaporation of water creates a slower, more insidious transient that has important safety consequences.

Evaporation of water creates a large steam volume that must be exhausted from the system. Since a pressure

DISCLAIMER

difference is required to overcome the flow-path resistances and drive this steam from the system, the internal pressure must adjust to create the required pressure difference. When the evaporation rate is high, the required pressure difference may cause the chamber pressure to increase above the ambient level. At pressures above ambient, leakage occurs from any leak paths in the equipment, possibly transporting hazardous and radioactive contaminants from the system. The waste-treatment facility would then become contaminated, a potentially serious health hazard for operations personnel would be created by the airborne contamination, and contaminants might be released to the environment. The quantification of such contaminant releases is important to meaningful safety analyses and is the end objective of an evaluation of this type of incident.

An inadvertent coolant-leakage incident occurred during *non*-radioactive operation of the Plasma Hearth Process (PHP) waste-vitrification development system at Argonne National Laboratory-West (ANL-W) when a stray electric arc ruptured the water-cooling jacket on the plasma torch positioning ram. Water was injected onto the surface of the approximately 1650 C (3002 F) molten waste pool and adjacent refractories. This pressurized the normally sub-atmospheric system above the ambient pressure for over 13 minutes, even though the water supply to the ruptured cooling jacket was quickly isolated, most other gas flows to the system were also shut down, and the exhaust fans on the off-gas system continued to operate.

A coolant leak in water-cooled equipment must be treated as an anticipated event. Although it had been accepted that a positive pressure could momentarily develop in the PHP from a coolant leak, the duration of the incident turned out to be much longer than had been expected. Similar pressurization in a radioactively contaminated system could have forced the release of contaminants from flanges, fittings, flexible boots, and other leak paths to the surroundings.

Despite the ostensibly leak-tight equipment envelope on the PHP and extensive searching for, and plugging, of leaks, careful pressure-decay testing of the system during qualification checkouts routinely measured leak rates of up to 9.4 l/min (0.33 ft^3/min), when the system was pressurized to just 254 mm of water column (10 in wc). It should be noted that an existing backup safety feature of the PHP installation at ANL-W is an independently ventilated and HEPA-filtered secondary-confinement enclosure, within which personnel are required to use protective respiratory equipment during operation. This secondary confinement would also have restricted any contaminants released to a limited area. It has been observed that some waste-treatment facilities are being proposed elsewhere with only the general facility boundary for secondary confinement.

An analysis of the thermal phenomena characteristic of coolant/hot-material interactions was undertaken to better understand this type of incident for reassessing the overall safety envelope of the PHP system and to provide guidance for operations-personnel safety, system design modifications, and environmental permitting. This paper identifies the key phenomena that need to be considered and describes the features of a comprehensive numerical model developed to analyze this type of incident. Additional analytic considerations are also discussed, and the numerical model is exercised in several examples to provide a better understanding of the physical behavior. Finally, the specific parameters and physical features of the reduced-scale PHP system installed at ANL-W were applied to the analysis model. The results were compared with some limited measurements made during the coolant-jacket-rupture incident in the PHP. These comparisons showed reasonably good agreement.

For realism, the formulation and examples used in this paper mimic many features of the PHP installation at ANL-W. However, the implications from this analysis apply equally to other systems, and the lessons learned should be examined in the safety evaluation of any waste-treatment technology that employs very high temperatures in water-cooled equipment. The analyses for coolant leakage in these systems would be similar to that for the PHP.

QUALITATIVE DESCRIPTION OF THE TRANSIENT

A high-temperature vitrification system is operating at normal conditions, processing waste. The base of the chamber might contain a molten waste pool, or may simply be a very high temperature, dry surface, e.g., such as in a secondary combustion chamber. Walls and ceiling of the chamber are refractory lined, with thicknesses typically varying from, perhaps, 25 mm to over 250 mm (1 to 10 in). Temperatures of the bare refractory surfaces may be up to 1500 C (2732 F), and any molten-waste-pool temperature may be as high as 1700 C (3092 F). The chamber boundary may have a cooling jacket (usually water) on the outer surfaces. Other components, such as torches, electrodes, viewing windows, etc. may also be water cooled. The internal pressure of the primary system is sub-atmospheric by some amount, typically from zero to up to, perhaps, negative 400 mm wc (-15.7 in wc) gage. At time zero, a cooling circuit ruptures and discharges coolant into the chamber.

Contaminant release rate is proportional to the internal pressure, the leak tightness of the system, and the

contaminant inventory, and is affected by the physical form of the contaminants. A necessary part of the contaminant-release quantification is therefore the prediction of the internal pressure of the system throughout the incident, in particular during the interval when the pressure is above the ambient level. The determination of this pressure response is the specific objective of the present study.

Prediction of the exact leakage characteristics is difficult. The size of the breach (coolant volume flow rate), the location of the breach, its orientation (which way is it "facing"), etc. can vary over a wide range. Does the coolant trickle into the chamber from behind the cooler side of the refractory, or does it make direct contact with the hot face? Does the coolant drip onto the surface, or is it sprayed? Does it pour onto the base of the chamber or first contact the walls and then run down? Such behavior of the coolant upon leaving the breach must be characterized for whatever rupture is hypothesized.

Evaporation of the leaking coolant is a complex heat-transfer phenomenon. Heat is transferred to the coolant by convection from surfaces directly contacted as well as by thermal radiation from other surfaces in the chamber. The higher the evaporation rate, the more steam that must be forced out of the system, and hence the higher will be the internal pressure.

Film boiling occurs when a relatively cool liquid contacts a very hot surface. This type of boiling creates a vapor blanket between surface and liquid that produces a surprisingly low heat-transfer rate, and thus a low evaporation rate. An example is the familiar *Leidenfrost Effect*, commonly observed when small droplets of water dance on contact with a hot pan and evaporate quite slowly. Because of this modest heat-transfer rate, the coolant leak rate may exceed the evaporation rate. This causes the coolant to accumulate in a pool in the lower part of the chamber. For leak rates greater than trickles, accumulation of a coolant pool turns out to be very likely despite the very high temperatures of the surfaces that the coolant contacts. *It is the formation of a pool of coolant and its subsequent evaporation that can maintain positive pressure in the primary system long after isolation of the leak source stops the coolant inflow.* The evaporation rate declines as the surfaces are cooled by heat transfer to the leaking coolant. Eventually, the vapor-generation rate is reduced to the point where the internal pressure falls back below the ambient level. This terminates the contaminant-release period, and further heat transfer eventually brings the system to a quiescent condition.

The terminal phase of any coolant leak is the formation of a pool of coolant on the base of the chamber. The model described in this study is based on the formation and behavior of such a pool, and the heat transferred to this pool over time determines the evaporation rate of the coolant. Once the evaporation rate is known, the pressure in the system can be calculated from knowledge of the hydraulic resistances.

Figure 1 depicts the components of a typical waste-treatment vitrification system. This system has been divided into two sections, the primary and the downstream, the former being the region from which release of contaminants may occur if pressurized above the ambient. Although the primary system may be comprised of several components, the pressure typically does not vary much among them, since the largest pressure losses are usually attributable to filters and off-gas air-pollution-control equipment in the downstream portion of the system. For simplicity, components in the primary system can be lumped into a single entity, and the temporal response of this lumped-primary-system pressure, $P_1(t)$, becomes a function only of the flow rate, temperature, pressure, and the flow resistances in the downstream piping and equipment. At quasi-steady conditions, the downstream flow rate is equivalent to the coolant evaporation rate.

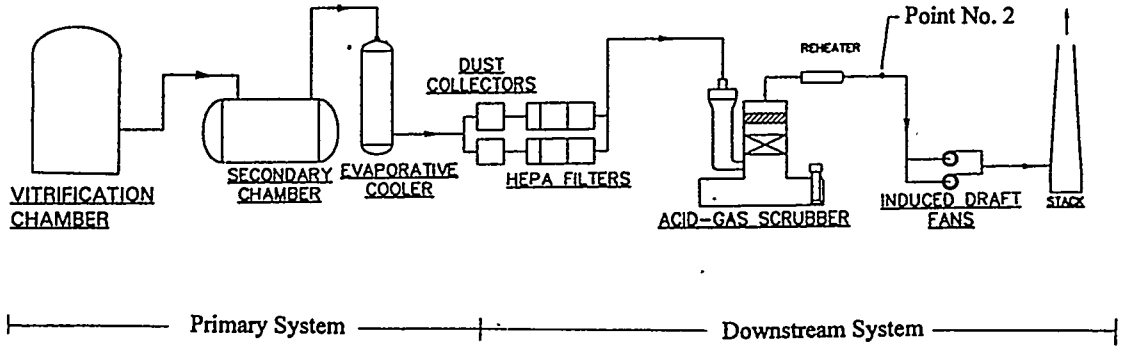

Figure 1. Typical Equipment Train in Waste-Vitrification Systems

The overall flow resistance is the sum of frictional losses, entry and exit losses, direction changes, constriction or expansion losses, and other turbulence-producing effects. Each of these is nearly proportional to $1/2*\rho v^2$, so that the overall pressure drop is also proportional to ρv^2, when v is based on some common cross-sectional flow area. Therefore the overall pressure drop can be written as

$$\Delta P \sim \frac{1}{2} \rho v^2 = G \rho v^2 \qquad (1)$$

G is a constant that depends only on the geometry and other physical characteristics of the off-gas equipment. Since G is a constant, the normal operating conditions for ΔP, v, and ρ can be used to deduce its value. This constant can then be used with the gas density that prevails during the coolant-leak incident (i.e., the density for steam plus whatever other gases are present) and the off-gas flow rate to determine the pressure drop during the incident. Since $\Delta P = P_1 - P_2$, where P_2 is some known downstream pressure, P_1 can then be determined.

LIMITING PRESSURE

The limiting evaporation rate clearly occurs when the coolant evaporates at the same rate that it flows into the system. This establishes the maximum pressure that *could* occur during this slow transient. The rate at which coolant flows into the system is not usually known, but can be estimated by comparing the cross-sectional area of the rupture, hypothetical or actual, to other flow cross-sectional areas in the affected cooling circuit. Using the rate at which coolant is normally being circulated in the ruptured loop just prior to the rupture is usually a good upper bound. Specification of the leak rate gives the evaporation rate, and with some knowledge of the temperature in the downstream system v in Eqn. 1 can be found, so ΔP can be computed.

Point No. 2 can be arbitrarily chosen, so long as the pressure at this point is known, and the constant G is evaluated relative to this same point. A convenient point is at the atmosphere where the stack discharges, but if any point downstream of the exhaust fan(s) is selected, the pressure created by the fans must be included in the resistance computation. For many installations, the pressure losses downstream of the induced-draft fan(s) are negligible, so P_2 can simply be set to the pressure developed at the fan inlet as deduced from the performance specifications for the fan.

Centrifugal fans have specific "head" vs. flow rate characteristics: for a given volume flow rate and fan speed, the head produced is fixed. So the actual fan pressure or, in this case, vacuum at the fan inlet is proportional to the mass density of the flowing fluid. The normal operation off-gas flow consists of mostly air, nitrogen, and combustion products such as CO, CO_2, NO, NO_2, and H_2O, together typically having an average molecular weight of about 30 in combustion systems. Since steam has a molecular weight of only 18, transition to steam flow reduces the vacuum at the fan inlet proportionately. This brings the pressure throughout the system closer to atmospheric, exacerbating the tendency for coolant evaporation to drive the primary-system pressure positive with respect to the ambient. For example, if the induced-draft fan creates a negative 635 mm wc (-25 in wc) gage pressure at its inlet in normal operation, the inlet pressure when exhausting the same volume flow rate of steam becomes only about negative 18/30*635 mm, or -381 mm wc (-15 in wc) gage.

Figure 2 shows the limiting peak pressure as a function of various hypothetical leak rates for a system having a resistance constant of 50 and for which the normal-operation value for P_2 is negative 635 mm wc (-25 in wc) gage. This curve has been computed from Eqn. 1 for flow of steam referenced to a 4-in Sch.-10 pipe at a downstream temperature of 204 C (400 F) and a local ambient pressure of 85 kPa (12.3 psia). It is seen that relatively high quasi-steady pressures can be created if complete, concurrent evaporation occurs at high leak rates. These are sustained pressures, in contrast to those that result from shock waves. By setting P_1 to the ambient pressure in Eqn. 1 the steam flow rate that just causes the primary pressure to reach the ambient value can be found. This flow is 178 kg/hr (391 lbm/hr), corresponding to a leak rate of 2.96 l/min (0.78 gal/min).

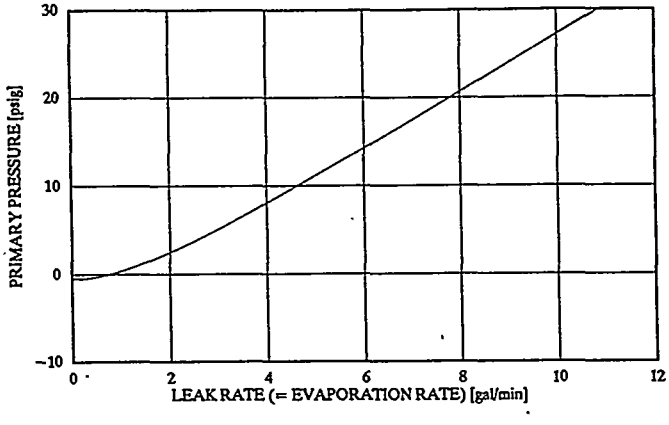

Figure 2. Limiting Peak Pressure for a Typical System With Specified Leak Rate, Ex. No. 1

There is a paradox that makes this limiting peak pressure unlikely to actually occur. Film boiling restricts the heat-transfer rate per unit surface area. If all of the leaking coolant is to be evaporated at its discharge rate and this is hypothesized to be as high as the normal circulation rate, very large areas of the hot refractory surfaces would need to be contacted simultaneously. To cover such large areas the coolant would have to be sprayed into the chamber. But in order to create a vigorous spray, back pressure across the rupture opening is needed. To achieve a strong back pressure the rupture size would need to be small, so the discharge rate would likely be less than the normal circulation rate.

TRANSIENT PRESSURE RESPONSE

The rate at which the hot surfaces can actually sustain evaporation needs to be considered to determine realistic pressures. Heat transfer to the leaking coolant also cools the hot surfaces, reducing the evaporation rate over time and causing the primary pressure to also decrease. A classic analytic solution can be applied to estimate a realistic peak pressure and the temporal response over the initial moments of the incident.

For very short periods of time the heat transfer to the coolant only affects the solid material within a few millimeters of its surface. The exact geometry of the region beyond that depth is therefore not important. Let the solid refractories be considered then to have infinite thickness. For the same reason, the refractory is presumed to be at uniform temperature, T_0, instead of having the falling gradient from hot face to back side that is more typical. (An analytic solution that includes the actual thickness and true temperature distribution can also be found, but the additional complexity is not warranted.) At time zero, the face of the refractory is exposed to a subcooled fluid whose saturation temperature is T_C with a constant convective-heat-transfer coefficient of h.

The analytic solution for the transient temperature response, $T(x, t)$, at any time t and depth x in the refractory for the conditions cited above is given by[1]

$$\frac{T(x,t) - T_C}{T_0 - T_C} = erf\frac{x}{2\sqrt{\kappa t}} + e^{\frac{h}{k}x + \left(\frac{h}{k}\sqrt{\kappa t}\right)^2} \cdot erfc\left[\frac{x}{2\sqrt{\kappa t}} + \frac{h}{k}\sqrt{\kappa t}\right] \qquad (2)$$

in which κ is the thermal diffusivity, erf is the error function, defined by

$$erf\, z = \frac{2}{\sqrt{\pi}} \int_0^z e^{-\lambda^2}\, d\lambda \qquad (3)$$

and $erfc\, z$ is the complimentary error function,

$$erfc\ z = 1 - erf\, z. \qquad (4)$$

In particular, the temperature response of the refractory surface is $T_S = T(0, t)$, where

$$\frac{T_S - T_C}{T_0 - T_C} = e^{\left(\frac{h}{k}\sqrt{\kappa t}\right)^2} \cdot erfc\ \frac{h}{k}\sqrt{\kappa t} \qquad (5)$$

Figure 3 depicts the analytic model.

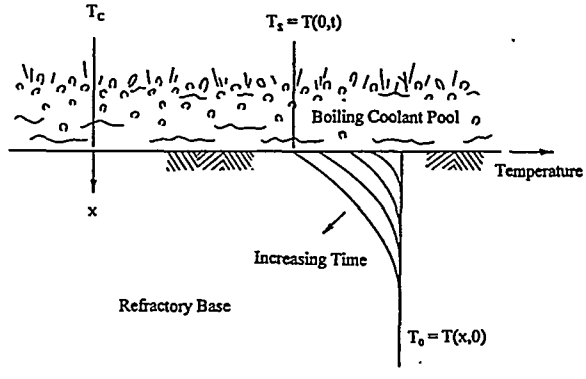

Figure 3. Pictorial Representation of the Analytic Model

The surface temperature can be used to compute the temporal convective heat flux to the coolant from

$$q_C(t) = h\left(T_S - T_C\right) \qquad (6)$$

The heat flux allows determination of the evaporation rate, using the temperature, enthalpy, and latent heat of evaporation for the coolant. This evaporation rate can finally be used to determine the temporal pressure in the primary by application of Eqn. 1. Mass-storage effects in the system are discussed later, but are ignored in this

quasi-steady analytic solution.

Thermal radiation from the walls and ceiling in the enclosure impose an additional heat load on the pooled coolant. Assume that the walls and ceiling are at a common temperature, T_W, and the coolant pool is boiling at its saturation temperature, T_C. The contribution from the radiant heat load can be readily assessed. Both refractories and water surface have very high surface emittance for radiation in the infrared. For simplicity here, these surfaces are therefore both assumed to be black. Because of the assumed flat base in the chamber, all radiation leaving the base impinges on the walls and/or ceiling. Under these conditions the radiant heat flux to the coolant pool, assumed to be evenly spread across the enclosure base, is simply

$$q_R = \sigma \left(T_W^4 - T_C^4\right) \tag{7}$$

For example, if the walls, ceiling, and base of the chamber are initially at the same temperature of 1093 C (2000 F) and the base is heating the saturated coolant pool with a convective film-boiling heat-transfer coefficient of about 284 W/m^2/C (50 BTU/hr/ft^2/F), per Reference No. 2, the ratio of radiant to convective heat-transfer rates to the pool is found to be

$$\frac{q_R}{q_C} = 0.7 \tag{8}$$

This ratio increases with increasing surface temperatures. This demonstrates that radiative heat transfer is of comparable magnitude to the convective rate, and therefore cannot be ignored. The radiant heat-transfer can be computed using Eqn. 7 for black bodies, or equations presented later for non-black surfaces, and added to the convective heat-transfer rate from Eqn. 6 to yield the total heat transfer for evaporation.

Results from this analytic solution will be compared to those from the numerical model in the following section.

NUMERICAL MODEL

The preceding development revealed several key facets that are important and must be properly accounted for in order to determine the primary-system-pressure response with reasonable realism. These are

a. likelihood that the coolant will collect in a pool at the bottom of the chamber;

b. radiation from the walls and ceiling to the pool surface; and

c. temporal cooling of the hot surfaces.

In addition, the calculation should account for possibly strong influences that result from

a. response of the coolant pool volume over time;

b. mass capacity within the system;

c. spatial variation of transport properties in the solids to account for different materials; and

d. temperature-dependent transport properties in the solids.

To include all of these effects, a numerical model of the chamber was developed and incorporated into the system hydraulic model. The physical heat-transfer model features three solid boundaries (ceiling, walls, and base), each discretized over its thickness. Heat transfer within the walls, ceiling, and base is one-dimensional, i.e., temperatures are uniform at a given depth. The coolant is presumed to pour into the chamber, contacting only the base, which consists of a flat, solid refractory base, possibly having a molten waste pool on top. Coolant discharge in excess of the evaporation rate is presumed to form a uniform-depth coolant pool on the base.

Appropriate initial temperatures are assigned to each node. The heat-transfer solution uses a forward-marching, explicit formulation over time increments chosen sufficiently small to maintain solution stability. For the results reported here a time increment of 0.36 s (0.0001 hr) was used during the rapidly changing conditions of the initial portion of the transient (the first 100 time steps, i.e., 36 s) and 3.6 s after the transient was well under way to reduce execution time and memory/storage requirements for the results tables generated.

Heat-transfer modes included in the calculation were intra-region conduction, including gap resistances, thermal radiation among the walls, ceiling, and pool (or base), boiling convection to the pooled coolant from the base, convection to the intact cooling jackets on the chamber boundary, and evaporation of the pooled coolant.

Neither natural convection in any viscous molten waste pool nor the release of its latent heat of fusion were considered in the results reported here, but those effects should have very little influence on the solution. Dynamic effects (gas acceleration) in the system should be negligible and were not included. Curvature in the walls is

included in the conduction calculations, but was omitted in these examples.

Mass-storage capacities for both the liquid pool and the primary system gas inventory are taken into account by application of continuity. The inventory of material at time t is M, and the response of M is described by

$$\frac{dM}{dt} = \dot{M}_{in} - \dot{M}_{out} \tag{9}$$

When applied to the coolant pool, M represents the accumulated pool mass, $\dot{M}_{in}$ is the coolant discharge rate from the rupture (user specified), and $\dot{M}_{out}$ is the evaporation rate, as determined by the thermal calculation.

For the gas phase, M represents the mass of gas within the system at any time, $\dot{M}_{in}$ is the evaporation rate, i.e., $\dot{M}_{evap}$, and $\dot{M}_{out}$ is the flow of gas out of the system. $\dot{M}_{out}$ is, of course, a function of the primary pressure and the downstream hydraulic resistances, pressure and temperature, as discussed before, so application of continuity becomes more complex when applied to the gas phase. This is further developed below.

Eqn. 9 can be re-cast from mass to pressure by application of a state expression. For simple gases at low pressure the ideal gas law provides an accurate equation of state:

$$PV = MRT \quad \text{or} \quad P = \rho RT \tag{10}$$

In a discretized form, the new primary-system pressure at the end of a time increment Δt is written as P_1', whereas the pressure at the beginning of the time increment is P_1. The flow of gas out of the primary system, $\dot{M}_{out}$, can be written as $\rho v A$, and v can be expressed in terms of ΔP from Eqn. 1. When these are combined with the state equation, continuity can be written as

$$P_1' = P_1 + \frac{RT}{V}\Delta t \left[\dot{M}_{evap} - A\sqrt{\rho \frac{\Delta P}{G}} \right] \tag{11}$$

To permit use of larger time increments, the average primary pressure during the time increment, $(P_1' + P_1)/2$, was used in Eqn. 11 for ΔP and in the determination of the gas density, ρ, from Eqn. 10. Normally this would yield an implicit formulation, but because the result is a quadratic equation in terms of the unknown primary pressure, P_1', it can be solved in closed form to yield the new pressure from

$$a\left(P_1'\right)^2 + b\,P_1' + c = 0 \tag{12}$$

in which

$$a = \left[1 - \frac{RTA^2}{4V^2G}\Delta t^2 \right]$$

$$b = -2\left[P_1 + \frac{RT}{V}\Delta t\,\dot{M}_{evap} \right] - 2\left(P_1 - P_2\right)\frac{RTA^2}{4V^2G}\Delta t^2$$

$$c = \left[P_1 + \frac{RT}{V}\Delta t\,\dot{M}_{evap} \right]^2 - \left[P_1^2 - 2P_1P_2 \right]\frac{RTA^2}{4V^2G}\Delta t^2$$

When a coolant pool exists, radiant heat transfer with the walls and ceiling is with the coolant surface; if no coolant has accumulated, or if the coolant pool has been consumed, the radiant exchange is among walls, ceiling, and base refractory of the chamber (or waste surface). Transmittance of the coolant pool to radiant energy is assumed negligible, and gases present in the chamber are presumed to be non-participating.

Radiant emission and reflection were assumed to be perfectly diffuse, and all surfaces were approximated as grey. Surface emittances are user defined. The total radiant heat-transfer rate to the coolant pool, $Q_R(t)$, was determined by simultaneous solution at each time step for the four surface radiosities, B_i (i = 1,4), from the four radiosity equations (one for each region - walls, ceiling, coolant pool, and base), each of the form[3]:

$$B_i = \epsilon_i E_{b_i} + \left(1 - \epsilon_i\right)\sum_{j=1}^{4} B_j F_{ij} \tag{13}$$

When the B_i have been found, the radiant heat-transfer rate from each surface is then computed as

$$Q_{R_i}(t) = A_i q_{R_i}(t) = A_i \left[B_i - \sum_{j=1}^{4} B_j F_{ij} \right] \qquad (14)$$

The solution approach used can be summarized as follows.

a. Specify physical dimensions of the chamber, including view factors among walls, ceiling, and base for radiant transport.

b. Discretize the walls, ceiling, and base into nodes across their respective depths.

c. Specify thermal transport properties for each node: specific heat capacity, thermal conductivity, density, surface emittance, and heat-transfer coefficients (all of which may be temperature dependent).

d. Specify initial node temperatures, the temperatures of the fluids in the respective cooling jackets, and temperature, enthalpy, and saturation temperature for the leaking coolant (the variation of these with pressure is negligible for the range of pressures applicable to this analysis).

e. Specify the initial primary pressure, $P_1(t=0)$ and the selected downstream pressure over time, $P_2(t)$. Evaluate the constant G consistent with the selection made for P_2.

f. Specify the applicable system volume and steam temperature in the downstream system (these need to be estimated in the current model, as discussed later; subsequent enhancements to the model are intended to analytically account for these).

g. Specify the profile for the coolant discharge from the ruptured circuit over time.

h. Compute the new node temperatures after a time increment Δt has elapsed.

i. Calculate the convective and radiant heat input to the coolant pool and its corresponding evaporation rate at this time.

j. Compute the new primary-system pressure, P_1', after this time increment from Eqn. 12.

k. Repeat steps h through j, above, by marching forward in time for the duration of the transient.

A special-purpose FORTRAN computer program named POOL was written to perform the calculation. The program was compiled and run on Ryan-McFarland FORTRAN, ver. 02.45.02, and execution was on an Intel Pentium II, DOS-based PC running at 233 MHZ. Results for various applications of this numerical model are presented and discussed in the following section.

RESULTS AND DISCUSSION

The steady operating temperatures just before the transient begins were computed on the basis of assumed surface and cooling-jacket operating temperatures. The capability to use temperature-dependent property values is built into the POOL program, but constant values were used for the examples presented here. Before examining the PHP incident, a few non-specific examples that exercise the numerical model and explore the physical behavior are presented.

Example No. 1 - Numerical Model Exercise

A system is running at a primary pressure of negative 83.8 mm wc (-3.3 in wc) gage. At time zero, a leak of water flows onto the base of the chamber at a constant flow rate of 1365 kg/hr, i.e., 22.7 l/min (3003 lbm/hr or 6 gal/min). Flow from the leak lasts for 1 min, representing a situation where an operator quickly detects, identifies, and isolates the leak source.

The back pressure, P_2, at the inlet to the induced-draft fan is negative 635 mm wc (-25 in wc) gage initially, and drops to negative 381 mm wc (-15 in wc) gage at the beginning of the transient, approximating the fan performance when transitioned to steam flow, as discussed earlier. All other gas flows are stopped at the onset of the transient.

The chamber is a simple dry, refractory-lined, water-jacketed, steel vessel, having a vertical cylindrical form with flat ceiling and base. Internal dimensions of the chamber are 864-mm (34 in) diameter and 1016-mm (40 in) high. The refractory construction is simple, consisting of a uniform layer of brick 152-mm (6-in) thick, having a thermal conductivity of 1.87 W/m^2/C (1.08 BTU/hr/ft/F) and a volumetric heat capacity of 2.5 MJ/m^3/C (38 BTU/ft^3/F). A 0.5-mm (0.020-in) thick air gap exists between the refractory and the steel vessel. The face temperatures of all surfaces initially are 1093 C (2000 F), and there is conduction to the cooling-jacket water at 38 C (100 F) with a convective heat-transfer coefficient of 454 W/m^2/C (80 BTU/hr/ft^2/F). Film boiling of the 38-C (100-

F) coolant water occurs at a constant heat-transfer coefficient of 284 W/m²/C (50 BTU/hr/ft²/F).[2]

The flow-resistance constant, *G*, is 50, the applicable system volume is 17 m³ (600 ft³), and the downstream temperature of the steam is assumed to be 204 C (400 F). All surfaces, including the surface of the coolant pool, were assumed to be black in this example.

The computed primary system pressure response is shown in Figure 4. The pressure rises very quickly to a peak of 5.05 kPa (0.73 psig) gage at 23.8 s after the start of the transient. The 23.8-s delay in reaching the peak pressure is the result of mass storage, i.e., this is the time during which pressure is building up in the system from the initial operating pressure. Following the sharp pressure rise, the pressure then begins to decay quickly as the heat-transfer rate to the pool decreases.

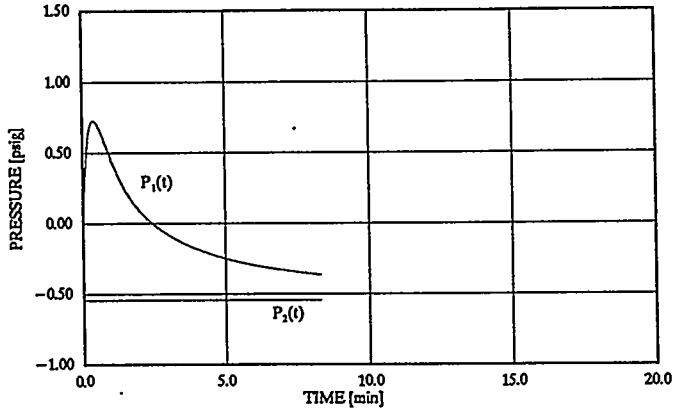

Figure 4. Primary-System Pressure Response, Ex. No. 1

The evaporation rate and coolant pool mass are shown in Figure 5 with the left-hand and right-hand ordinates, respectively. The evaporation rate is 399 kg/hr (878 lbm/hr) initially, significantly less than the leak rate of 1365 kg/hr (3003 lbm/hr), and drops off quickly as the chamber surfaces cool. This creates a rapidly increasing pool of coolant over the first minute of the transient, reaching 17.3 kg (38 lbm) by the time the leak source is isolated. The coolant pool then begins to be depleted at a decreasing rate, reflecting the decreasing evaporation rate generated by the constantly cooling surfaces. The response of the coolant pool mass is shown on a larger scale in Figure 6.

Evaporation continues at a sufficiently high rate to maintain the primary at positive pressure until about 2.5 minutes. Thereafter, the lower evaporation rate allows the primary to return to negative pressure with respect to the ambient. By 8.3 minutes the accumulated pool of coolant has been completely evaporated. At this time, the chamber base surface temperature is still nearly 250 C (482 F), indicating that the coolant pool continued to be in a film-boiling mode throughout the evaporation period.[2]

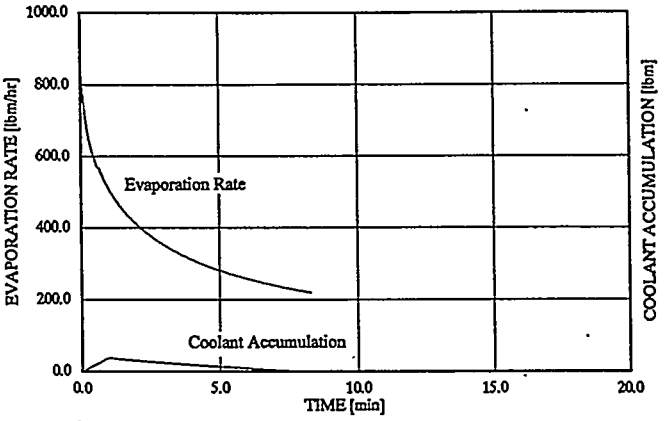

Figure 5. Coolant Evaporation Rate and Pool Mass Response, Ex. No. 1

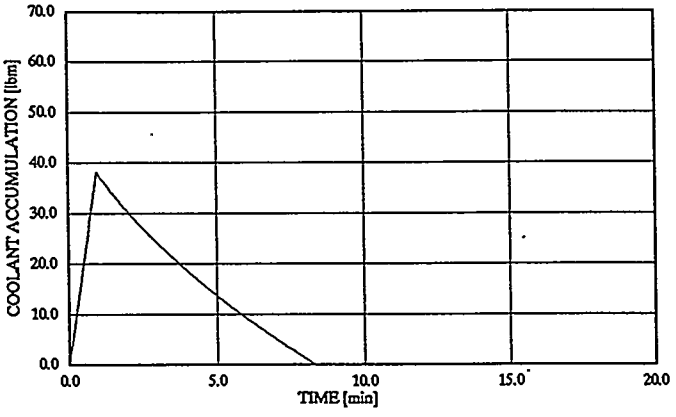

Figure 6. Coolant Pool Mass Response, Ex. No. 1

Figure 7 shows the heat transfer to the coolant pool by convection from the chamber base and by radiation from the walls and ceiling. The convective heat-transfer rate is greater initially, but is rapidly reduced as the base refractory is cooled by the pool. The walls and ceiling are also cooling, of course, but more slowly since together they have much more mass than does the base.

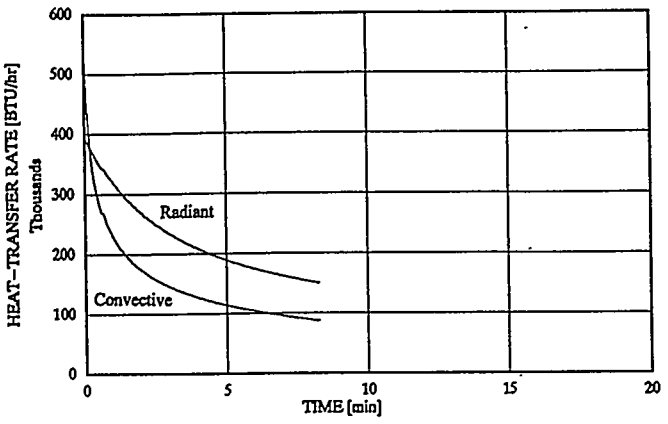

Figure 7. Convective and Radiant Heating of the Coolant Pool, Ex. No. 1

Example No. 2 - Mass Storage Effects and Comparison of the Numerical Computation to the Analytic Solution

This example first explores the impact of mass storage per the development from Eqn. 9. All parameters were the same as those in Example No. 1, except as noted.

Figure 8 shows the pressure response from Example No. 1, which had a system volume of 17 m^3 (600 ft^3), along with similar results calculated with system volumes of 34, 5.7, and 0.28 m^3 (1200, 200, and 10 ft^3), respectively.

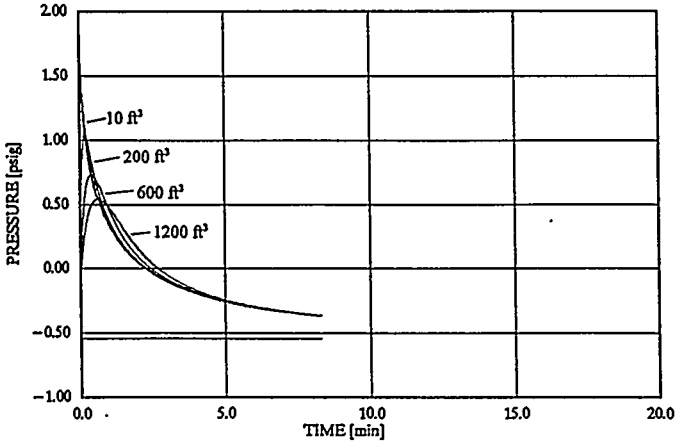

Figure 8. Effect of Mass-Storage on the Primary-System-Pressure Response

The larger the volume is the lower is the peak pressure developed, because the evaporation rate is rapidly decreasing during the time that is required to pressurize the system, as seen in Figure 5. There is less importance in including the mass-storage effect for the smaller-volume systems. For the conditions applicable to this example, mass storage is negligible for the 0.28-m^3 (10-ft^3) system, and the results that would have been found by simply letting $\dot{M}_{out}$ equal $\dot{M}_{evap}$ (i.e., setting dM/dt equal to 0 in Eqn. 9) differ negligibly from those shown. Since there is no feedback from continuity, the results for the evaporation rate and coolant pool mass are independent of the system volume.

Mass storage is tacitly ignored in the closed-form analytic solution presented in Eqn. 2, so comparison can only be made to results from the numerical model having the 0.28-m^3 (10-ft^3) volume. The pressure responses are shown in Figure 9. The chamber floor area of 0.59 m^2 (6.31 ft^2) is applied to the sum of heat fluxes determined by Eqn. 6 and the radiant heat transfer calculated by application of Eqn. 7 (since blackbody radiation has been specified in this example).

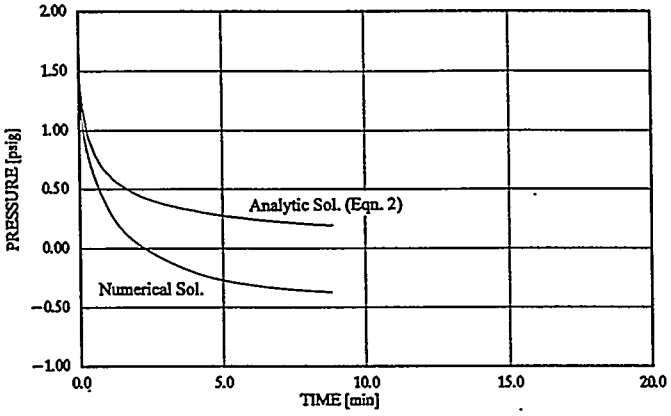

Figure 9. Comparison of Primary Pressure Responses from Analytic and Numerical Solutions, Ex. No. 2

As expected, the analytic result matches the numerical result initially, but then the pressure falls more slowly as time increases. This results from two factors: 1) the radiant heat-transfer rate remains higher in the analytic solution as a result of the assumed constant-temperature walls and ceiling; and 2) the higher interior temperatures in the base refractory inherent in the uniform-initial-temperature analytic solution. When the cooling of the walls and ceiling is suppressed in the numerical model by fictitiously increasing their heat capacities 1000 times, enough to maintain surface temperatures within 1 degree of their initial values, the first of these factors is eliminated, and the divergence between the calculations is much less, as shown in Figure 10. Finally, specifying the same uniform initial temperature in the base as in the analytic case - 1093 C (2000 F) - eliminates the second factor, and the numerical solution is found to be coincident to that

from the analytic solution. Conformance of the pressure responses from these two models provides at least a partial validation of the numerical model.

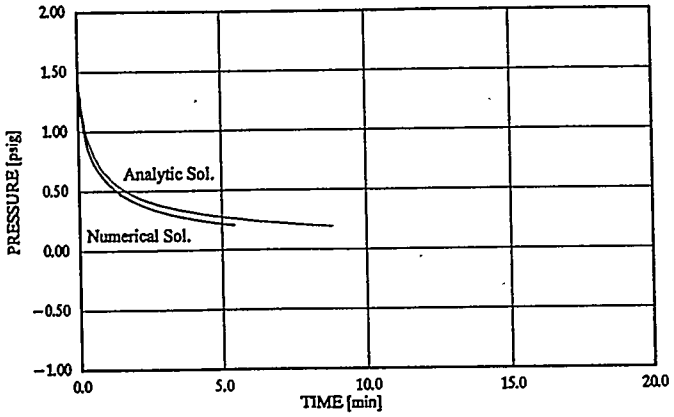

Figure 10. Primary-System Pressure Responses from Analytic and Numerical Solutions, with Constant Wall & Ceiling Temperatures, Ex. No. 2

Example No. 3 - PHP System Leak-Incident Evaluation

Within the constraints of the many simplifications built into the present numerical model, a best estimate is made for the predicted response of the PHP system at ANL-W to compare to the pressure that was measured during the leak incident. The PHP vitrification chamber is depicted in Figure 11.

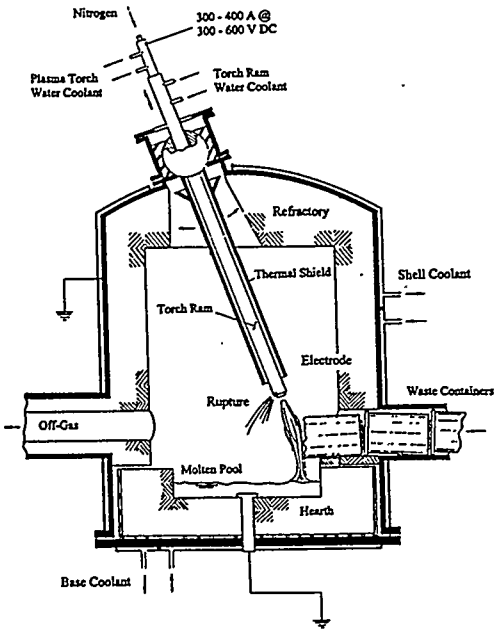

Figure 11. Vitrification Chamber Configuration in the PHP System at ANL-W

The applied coolant-leak profile is shown in Figure 12. No instrument signals were recorded that could provide the exact leak rate nor the duration of the main coolant leak. An initial leak rate equal to the normal circulation rate of 22.7 l/min (6 gal/min) was used in the analysis for the approximately 1.6 cm^2 (0.25 in^2) rupture that occurred in the torch ram jacket. It was estimated that the operator isolated the ruptured cooling circuit between two and three minutes after the incident began. Therefore, a duration of 2.5 min was used in the calculation. It will be seen shortly that, for this specific situation, the exact leak rate and the duration of this period are of only minor importance to the most interesting results from the analysis.

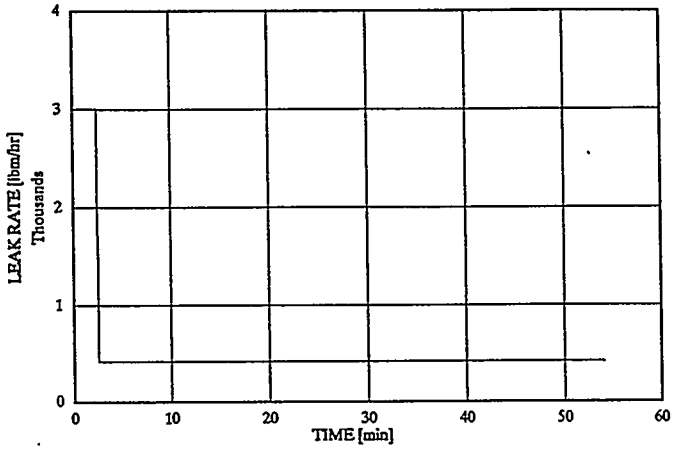

Figure 12. Hypothesized Coolant Leak-Rate Profile for the PHP Leak Incident, Ex. No. 3

A downstream check valve on the ruptured coolant circuit apparently failed to seat properly when the ruptured circuit was shut down. This caused coolant from intact cooling loops that remained active to flow into the vitrification chamber through the breach even after the water supply to the faulty loop had been valved out. All coolant loops were eventually shut down about 4 hr following the start of the leak incident. Subsequent inspection revealed 379 l (100 gal) of water in the primary system. If it is estimated that perhaps twice this much actually leaked into the system (i.e., 50% was assumed to have been evaporated in the vitrification and secondary combustion chambers during the 4-hr period) then the average flow rate of this slow leak would have been about 190 kg/hr (417 lbm/hr). Again, the exact value for this long-term leak will be found to have only a minor role in the results for this particular case.

Numerous compressed gases flow into the PHP system during normal operation. These include the nitrogen from which the plasma is generated, nitrogen

gases used for local cooling of viewports, air for processing combustible waste materials, propane and air for maintaining the off-gas temperature in the secondary combustion chamber, air for atomization of a water spray for attemperation of the off-gas in the evaporative cooler, and a nitrogen purge on the waste-feed magazine for cooling. Except for the feed-magazine purge, these gas flows were automatically shut down upon detection of the low pressure in the ruptured coolant loop.

The specification of $P_2(t)$ in this case was not simple. The proportions of nitrogen and steam vary in the off-gas. Furthermore, one of the two parallel induced-draft fans was shut down briefly for inspection after the first few minutes when moisture was observed to be leaking from the fan's casing. So for this calculation, a table of the measured pressure at a point just downstream of the reheater (point No. 2 in Figure 1) was used to define $P_2(t)$.

The refractory structure in the PHP is typical of an actual installation, and is much more complex than that used in the previous example. Figure 13 shows the dimensions and other features of the PHP refractory and the node structure used in the numerical model. Thermophysical property values used are given in Table 1.

The drop in pressure between the PHP primary system and the downstream point is gradual, since the air-pollution-control equipment consists of a three-unit HEPA-filter train, venturi scrubber, packed-bed scrubber column, reheater, and ducts. During the transient the pressure in these components increases to some intermediate values between that of the primary system and the downstream point. To account for mass storage in these components a linear decrease in pressure between the primary system and point No. 2 was assumed. The system volume used was therefore that of the primary plus one-half of the remaining volume, giving an effective system volume for the calculation of $2.1 + \frac{1}{2} * 5$ m^3, or 4.6 m^3 (162 ft^3). As was seen in Example No. 2 (Figure 8), however, the accuracy of this assumption is not very important, because mass-storage has only a small effect for system volumes this small.

Ceiling

Initial Temperatures	Thicknesses	Material
A. 1800 F	A-B 9.5 in	Blu-Ram Refractory
B. 275 F	B-C 0.020 in	Nitrogen Gap
C. 142 F	C-D 0.5 in	Steel
D. 140 F		

Walls

Initial Temperatures	Thicknesses	Material
A. 2200 F	A-B 4.5 in	Mullite Refractory
B. 1667 F	B-C 0.020 in	Nitrogen Gap
C. 1512 F	C-D 1.5 in	K-30 Insulating Refractory
D. 299 F	D-E 0.020 in	Nitrogen Gap
E. 143 F	E-F 0.5 in	Steel
F. 140 F		

Base

Initial Temperatures	Thicknesses	Material
A. 3000 F	A-B 0.5 in	Molten Waste
B. 2993 F	B-C 3 in	Ruby Rammable Refractory
C. 2679 F	C-D 0.020 in	Nitrogen Gap
D. 2468 F	D-E 3 in	Ruby Brick Refractory
E. 2106 F	E-F 0.020 in	Nitrogen Gap
F. 1896 F	F-G 1 in	K-30 Insulating Refractory
G. 794 F	G-H 0.020 in	Nitrogen Gap
H. 583 F	H-I 1 in	Steel
I. 576 F	I-J 0.040 in	Nitrogen Gap
J. 155 F	J-K 2 in	Steel
K. 140 F		

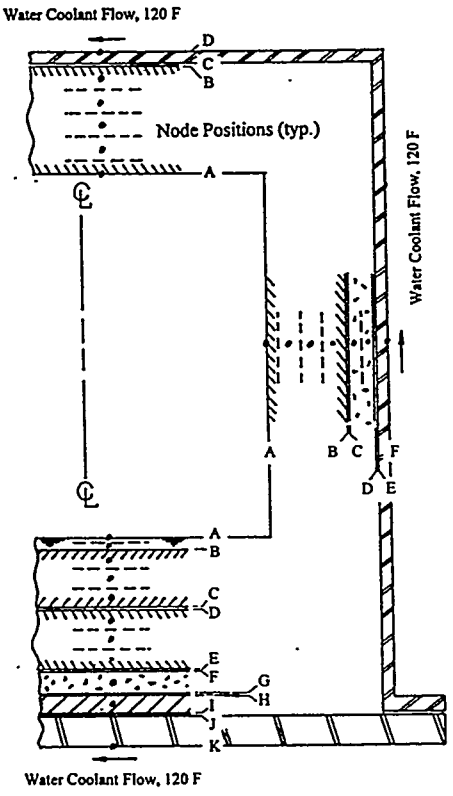

Figure 13. Dimensions, Materials, Node Arrangement, and Initial Temperatures for the PHP Model, Ex. No. 3

The calculated pimary system pressure response is shown in Figure 14. As in the previous example, the pressure initially rises rapidly as the very hot surfaces evaporate the coolant, reaching a maximum of 22.1 kPa gage (3.2 psig) at 20 s. Then, as the surfaces are cooled by the leaking water, the pressure gradually falls back, showing the momentary interruption in its decay in concert with the imposed downstream pressure variation at about 7 min. After 12.6 min the primary pressure once again becomes sub-atmospheric.

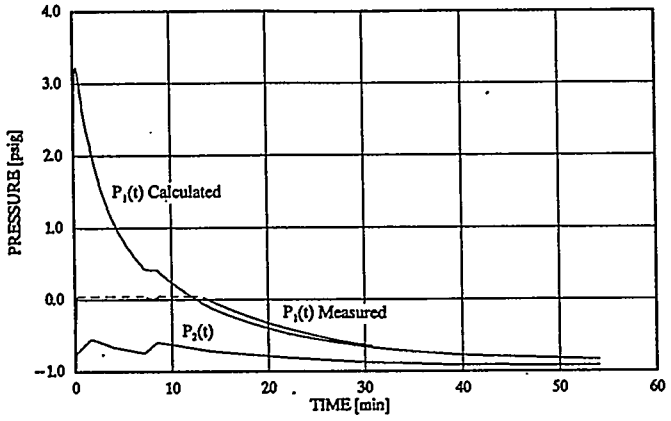

Figure 14. Comparison of the Calculated Primary Pressure to the Measured Pressure in the PHP Leak Incident, Ex. No. 3

The second curve on this figure is a replication of the measured chamber pressure during the transient. The pressure that occurred exceeded the high limit of the instrument range, 25-mm wc (1-in wc) gage, shortly after zero to about 13 min. It is known that the incident raised a relief valve that was set at positive 381-mm wc (15-in) gage (albeit uncalibrated). Extrapolating the measured response in the region where the pressure was off-scale suggests that the actual peak pressure was probably less than the calculated peak pressure of 22.1 kPa gage (3.2 psig) computed with the numerical model. The downstream pressure dip at about 7 min almost caused the measured primary-system pressure to momentarily return to sub-atmospheric (although this is barely visible in the ordinate scale of Figure 14). It would appear that the actual peak pressure developed was about 7 kPa-gage (1 psig). The measurement showed that the primary returned to subatmospheric pressure about 13.6 minutes after the incident began.

The most probable explanation for the discrepancy in the peak pressures is that the current numerical model does not account for the central, 610-mm (24-in) diameter molten waste cavity in the PHP hearth. Had the coolant pool been restricted to this cavity rather than assumed to have been spread evenly over the entire 864-mm (34-in) diameter base, both the convective and the radiant heat-transfer rates would have been reduced by a factor of about two. The numerical model is being refined to include this and other effects.

The lower actual peak pressure may have also been influenced by the developing conditions of rupture geometry and leak orientation that existed during the first few seconds of the event, in contrast to the step changes used in the model. At longer times after the start of the incident, the numerical model shows a pressure recovery that is slightly faster than the measured pressure. Overall, the agreement is satisfactory, considering all of the uncertainties that exist. The agreement is helped, of course, by the use of the measured downstream pressure for $P_2(t)$, as this removes one potential source of error from the calculation.

The higher calculated pressure during the initial portion of the transient together with the lower calculated pressure during the latter part are consistent. Higher pressures initially imply a greater evaporation rate, and when this occurs early on heat is removed from the refractory that would otherwise be available for evaporating the coolant pool later.

The evaporation rate is shown in Figure 15. As in the previous example, the evaporation rate is well below the initial rate of 1365 kg/hr (3003 lbm/hr) that the coolant is flowing into the chamber, causing an immediate accumulation of a coolant pool.

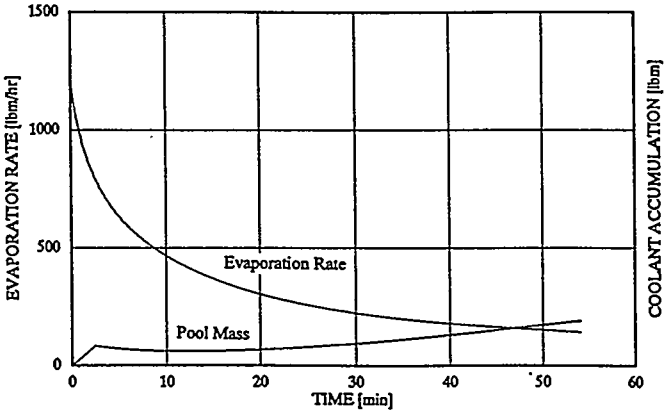

Figure 15. Coolant Evaporation Rate and Pool Accumulation in the PHP Leak Incident, Ex. No. 3

The coolant pool mass is shown in Figures 15 and 16. The response of the pool volume (mass) in the early part of

the transient is similar to that in the previous example, increasing rapidly while the leak is active, then beginning to decrease as the high evaporation rate depletes the pool. In this case, however, the continuing influx of leaking coolant at the lower rate prevents the complete consumption of the pool. After about 12.3 min the chamber surfaces have been sufficiently cooled that the evaporation rate drops below that of the long-term leak rate. Thereafter, the accumulated mass of coolant begins to slowly increase again, reaching 86.8 kg, or 86.8 l (191 lbm or 22.9 gal) after 54 min (the end of the calculation), eventually producing the residual water mass later discovered in the system.

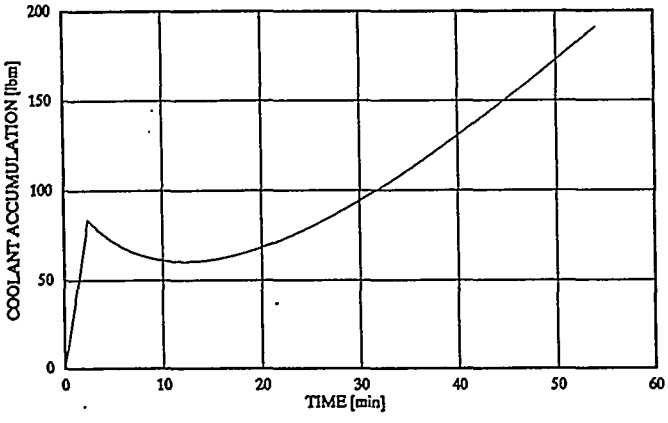

Figure 16. Coolant Accumulation in the PHP Leak Incident, Ex. No. 3

Surface emittance used for radiant heat transfer were 0.9 for the refractories and 0.95 for the coolant pool surface. Figure 17 shows how the radiative and convective heat-transfer rates to the coolant pool varied over time. In this case, the convective heat-transfer rate remained higher than the radiant heat-transfer rate for an extended period, owing to the much higher initial temperature of the base as compared to the walls and ceiling. After 27.5 min the radiant heat transfer becomes greater than the convective rate. The surface temperatures of the base, walls, and ceiling at this time are 322 C, 784 C, and 767 C (612 F, 1444 F, and 1412 F), respectively.

SUMMARY AND CLOSURE

A thermal model that included the major features associated with an analysis of coolant-leak incidents into very high temperature enclosures was developed. The key feature was the likely formation of a pool of coolant, whose evaporation over time strongly influences the pressure history of the system long after the coolant leak has been isolated. The recognition of the influence of steam flow on the pressure (vacuum) performance of the induced-draft fans during this type of incident and the inclusion of transient thermal radiation from non-contacted surfaces were other important features in the analysis.

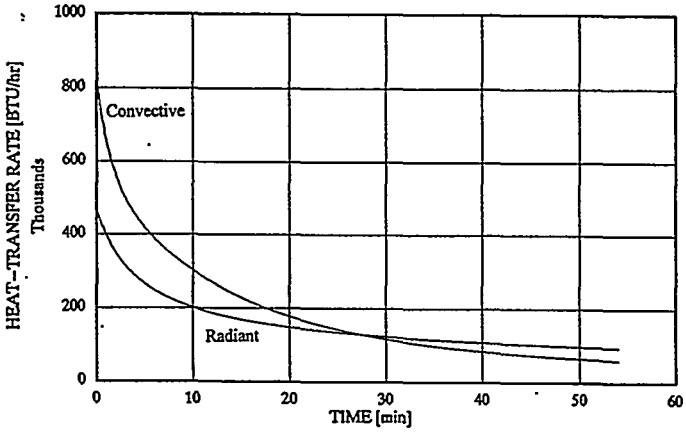

Figure 17. Convective and Radiant Heat Transfer to the Coolant Pool in the PHP Leak Incident, Ex. No. 3

There are numerous potential influences that can affect the calculated pressure response. The event addressed here is driven by a complex set of heat-transfer phenomena, taking place at very high temperatures, and, of course, the model used here is an idealization. Considerations that could affect the comparison are listed below.

a. Knowledge of thermal and transport property values at very high temperatures is poor; for example, thermo-physical properties of the molten waste could only be guessed, using an average of the properties for equal masses of iron and silica, the major constituents.

b. The 610-mm (24-in) diameter central cavity in the PHP base, the "corners", and the true radiosity distributions introduce two-dimensional effects that have not been included in the numerical model.

c. The quantity of molten waste in the hearth is important; thicker layers give the same peak pressure (because the heat-transfer area is unchanged), but produce longer positive-pressure durations because of the high heat capacity and thermal conductivity of this material compared to those for refractory. The 12.7-mm (0.5-in) thick molten-waste layer used in Example 3 corresponded to the 20 kg (44 lbm) of waste estimated to have been in the PHP hearth cavity when the rupture occurred.

d. There is considerable uncertainty as to the actual hydraulic behavior of the leak; the cooling-circuit rupture obviously did not instantly reach its final size and shape, and during this time the flow rate and flow pattern emanating from the breach were unknown.

e. The off-gas flow was assigned a uniform temperature along its flow path, (the actual temperature is strongly affected by flow through the evaporative cooler, wet scrubber, and reheater).

f. Condensation in the wet scrubber was not included, although much of the pressure loss has already occurred by this point.

g. The primary system components have been lumped into a single entity having uniform temperature and pressure.

h. The most significant part of the transient occurs when there exist very large differences between the hearth surface temperature and the coolant saturation temperature, causing film-type boiling, for which appropriate convective heat-transfer coefficients are not well known.

Still, the comparison of the calculated pressure response to that of the measured pressure shows sufficiently good agreement in terms of the positive-pressure duration that a judicious application of contaminant-release calculations based on these pressures would be useful. Such predictions should be used only as a guide and applied very conservatively.

Table 1

Thermophysical Properties for the PHP Analysis - Example No. 3

Material	Thermal Conductivity W/m/C *(BTU/hr/ft/F)*	Specific Heat Capacity J/kg/C *(BTU/lbm/F)*	Mass Density kg/m^3 *(lbm/ft^3)*
Steel	47.9 *(27.7)*	460 *(0.11)*	7700 *(480)*
Mullite Refractory	2.16 *(1.25)*	1005 *(0.24)*	2566 *(160)*
K-30 Insulating Refractory	0.317 *(0.183)*	1674 *(0.4)*	818 *(51)*
Blu-Ram	1.37 *(0.792)*	1005 *(0.24)*	2566 *(160)*
Ruby Ram	13.3 *(7.67)*	628 *(0.15)*	3144 *(196)*
Ruby Brick	2.89 *(1.67)*	670 *(0.16)*	3144 *(196)*
Molten Waste	25.4 *(14.7)*	753 *(0.18)*	5133 *(320)*
Gap	0.033 *(0.019)*	0	N/A

NOMENCLATURE

English Symbols

A	area
B	radiosity
a	definition, per Eqn. 12
b	definition, per Eqn. 12
c	definition, per Eqn. 12
E	radiative emissive power
F	view factor
G	constant, defined by Eqn. 1
h	heat-transfer coefficient
k	thermal conductivity
M	mass
$\dot{M}$	mass flow rate
P	pressure
Q	heat flow rate
q	heat flux
R	gas constant
T	temperature
t	time
x	position as measured from surface

V	volume
v	scalar velocity
z	indefinite symbol

Greek Symbols

Δ	indicator of a difference
ϵ	surface emittance
ρ	mass density
κ	thermal diffusivity
λ	integration constant
σ	Stefan-Boltzmann constant, 5.6688E-8 $W/m^2/K^4$ (0.17141E-8 $BTU/hr/ft^2/R^4$)

Subscripts

b	denotes blackbody
C	coolant
$evap$	evaporation
i	specific entity
j	specific entity
in	in[to]
out	out [of]
R	thermal radiation
S	surface
W	wall
0	initial condition
1	primary point
2	downstream point

ACKNOWLEDGMENT

This work was supported by the U. S. Department of Energy Environmental Management and Restoration, EM-50, through the Mixed Waste Focus Area, TTP CH2-3-MW-51.

REFERENCES

1. H. S. Carslaw and J. C. Jaeger, *The Conduction of Heat in Solids*, Sec. 2.7, 2nd Ed., Oxford Press, 1959.

2. E. A. Farber and R. L. Scorah, "Heat transfer to boiling water under pressure," *Trans. Am. Soc. Mech. Eng.*, 70, p.369, 1948.

3. E. R. G. Eckert and R. M. Drake, Jr., *Analysis of Heat and Mass Transfer*, Sec. 15.2, McGraw-Hill Book Company, New York, 1972.